

# Spin-Orbit Interaction Enabled High-Fidelity Two-Qubit Gates

Jiaan Qi,<sup>1,\*</sup> Zhi-Hai Liu,<sup>1,†</sup> and H. Q. Xu<sup>1,2,‡</sup>

<sup>1</sup>Beijing Academy of Quantum Information Sciences, Beijing 100193, China

<sup>2</sup>Beijing Key Laboratory of Quantum Devices, Key Laboratory for the Physics and Chemistry of Nanodevices, and School of Electronics, Peking University, Beijing 100871, China

(Dated: September 8, 2023)

We study the implications of spin-orbit interaction (SOI) for two-qubit gates (TQGs) in semiconductor spin qubit platforms. The exchange interaction governing qubit pairs is anisotropic under SOI, posing a problem for conventional TQGs derived under the Heisenberg exchange. After developing a concise form of the effective two-qubit Hamiltonian with SOI, we use it to derive properties of TQGs in the rotating-frame. Two main observations are made. First, in contrary to past belief, we find that an appropriate amount of SOI can enhance the controlled-phase gate fidelity compared to the no-SOI case. Second, SOI enables novel two-qubit dynamics, that are conventionally inaccessible through DC evolution, such as the reflection gate and the controlled-not gate.

Semiconductor spin qubits are promising candidates for large-scale, fault-tolerant quantum computers due to their potential in scalability and miniaturization in physical size [1]. In this scheme, quantum dots defined in semiconductor devices are commonly used to trap electrons or holes, whose spin states are employed to host quantum information [2]. Currently, high-speed and precise manipulation of single-qubit states is dominantly achieved using radio-frequency electric signal [3–6]. The physical principle behind this technique is spin-orbit interaction (SOI), a key mechanism derived from the relativistic Dirac equation and responsible for many novel effects such as the spin Hall effect [7], spin transistors [8], and Majorana states in superconducting nanowires [9–12].

Strong SOI is generally desirable for single-qubit gates for enabling high-speed operation [13, 14]. The role of SOI and its influence in two-qubit gates (TQGs) are, however, less straightforward. Standard treatments for the exchange induced TQGs are based on the spherically symmetric Heisenberg interaction [15, 16]. While it has long been understood that SOI gives rise to *anisotropic* exchange coupling, possessing only axial symmetry [17–21]. The anisotropic component of exchange coupling is typically small in bulk materials [17], but could be comparable to the isotropic part in low-dimensional semiconductor structures [18, 20]. This complexity introduced by SOI is often dismissed in the seminal works on spin qubits. However, since high-fidelity multiple-qubit gates, which are fundamental to fault-tolerant quantum computing, have become increasingly relevant, the prospect of a potential loss in fidelity demands urgently for a clearer understanding of the effects of SOI [22–24]. Much research interest has been drawn to this issue. The primary perspective considers the anisotropic deviation as a source of errors in TQGs. Schemes to alleviate the “anisotropy errors” have been proposed, typically involving tailoring the control pulses and/or the parameters of the exchange interaction [25–31]. Another approach is to acknowledge the inevitability of the anisotropy effects of SOI and build new sets of TQGs that intrinsically ac-

counts for these effects [32–35]. Both of these approaches require extra resources to account for SOI. These overheads increase system complexity and may introduce additional control errors by themselves.

In this Letter, we take an alternative approach in which SOI is naturally incorporated into TQGs without the need for extra error alleviation or for introducing new quantum logics. In fact, SOI enables direct high-fidelity implementation of the controlled-phase (CPhase) gate, with fidelity surpassing the non-SOI case. Other SOI-enabled high-fidelity gates, such as the reflection gate and the controlled-not (CNOT) gate are also possible following our formalism. Made possible by a combination of improved theoretical understanding and experimental control, our direct approach shows the new possibilities by proper utilization of SOI in spin qubit platforms.

Our physical setup is a double-quantum-dot (DQD) made in a semiconductor nanostructure with strong SOI. For brevity concerns, electron motion within the DQD system is assumed to be restricted to the direction defined along the dots. As illustrated in Fig. 1 for a nanowire

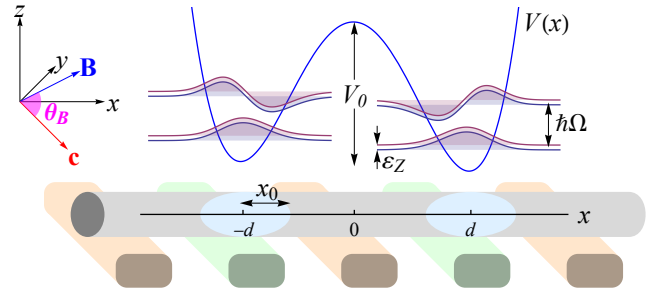


FIG. 1. Schematic illustration of a model two-spin qubit device defined in, e.g., a semiconductor nanowire with strong SOI via a finger-gate technique. The electrostatic potential profile (in blue) and the first 8 low-lying single-electron states staggered by their energy levels are illustrated on top. The top-left inset shows the reference frame and the angle  $\theta_B$  defined between magnetic field  $\mathbf{B}$  and the SOI vector  $\mathbf{c}$ .

DQD as example, a set of barrier and plunger gates is employed to define a double-dot potential  $V(x)$  with minima located at  $x = \pm d$ . The DQD is maintained in a low-energy state, electrically depleted to contain two electrons only and subject to a static and possibly inhomogeneous magnetic field  $\mathbf{B}(\mathbf{r})$ . The dot separation is large enough  $d > x_0$  such that the orbital states are well-localized. Here,  $x_0 \equiv \sqrt{\hbar/m_e^* \Omega}$  is the Bohr radius of the dots with characteristic frequency  $\Omega$  and electron effective mass  $m_e^*$ . The characteristic barrier height  $V_0 \gg \hbar\Omega$  allows multiple bounded orbits in each dot. Finally, the orbital energy  $\hbar\Omega$  prevails over the Zeeman energy  $E_Z$  and the detuning  $\varepsilon \equiv V(-d) - V(d)$ . No particular detail of the potential is otherwise required.

In general, SOI can consist of the Rashba and the Dresselhaus terms. For the one-dimensional geometry, the coupling Hamiltonian takes on a simple form:  $H_{\text{SO}} = \alpha p_x \sigma_c$ , with the SOI strength  $\alpha$  and the Pauli operator  $\sigma_c = \hat{\mathbf{c}} \cdot \boldsymbol{\sigma}$  defined along a vector  $\hat{\mathbf{c}}$  determined by SOI. Presence of SOI modifies many defining aspects of the spin qubit. The spin direction is recognized in the “spin frame”  $(\hat{\mathbf{a}}, \hat{\mathbf{b}}, \hat{\mathbf{c}})$ , in which we have the Zeeman Hamiltonian  $H_Z = E_Z/2 (\cos \theta_B \sigma_c + \sin \theta_B \sigma_a)$ , where  $\theta_B$  denotes the angle between  $\mathbf{B}$  and  $\hat{\mathbf{c}}$  and  $E_Z \equiv g\mu_B |\mathbf{B}|$  with  $g$  being the Langé-g factor  $g$  and  $\mu_B$  the Borh magneton. A single-dot system in presence of strong SOI can be solved perturbatively [14]. The quantization energy reduces to  $\varepsilon_Z = f_{\text{so}} E_Z$ , for  $f_{\text{so}} \equiv \sqrt{\cos^2 \theta_B + e^{-2(x_0/x_{\text{so}})^2} \sin^2 \theta_B}$ . The qubit states also become entangled in spin and orbital parts,

$$|\uparrow/\downarrow\rangle \simeq \cos(\vartheta/2) |0_{\pm}\rangle |\uparrow/\downarrow\rangle \pm \sin(\vartheta/2) |0_{\mp}\rangle |\downarrow/\uparrow\rangle, \quad (1)$$

where  $|0_{\pm}\rangle \equiv e^{\pm i \hat{x}/x_{\text{so}}} |0\rangle$  are the momentum-displaced orbital ground states, with the spin-orbit length  $x_{\text{so}} = \hbar/m_e^* \alpha$ , and the mixing angle  $\vartheta \equiv \arccos(\cos \theta_B / f_{\text{so}})$ .

One can apply the Hund-Mülliken theory to derive the low-energy Hamiltonian of the DQD system [36]. Linear combination of states (1) at each local dot leads to an energetically-truncated basis  $|\Phi_{L\downarrow}\rangle, |\Phi_{L\uparrow}\rangle, |\Phi_{R\downarrow}\rangle, |\Phi_{R\uparrow}\rangle$ , where the subscript L/R indicates state localized to the left/right dot. Using the creation/annihilation operators  $a_{j\sigma}^\dagger/a_{j\sigma}$  for the state  $|\Phi_{j=L,R,\sigma=\uparrow,\downarrow}\rangle$ , we can write the Hamiltonian as a sum of the dot term  $H_d = \sum_j (\varepsilon_j + \varepsilon_{Z,j}) n_{j\uparrow} + (\varepsilon_j - \varepsilon_{Z,j}) n_{j\downarrow}$ , the tunnelling term  $H_t = \sum_{\sigma} (t_{\sigma\sigma} a_{L\sigma}^\dagger a_{R\sigma} + t_{\sigma\bar{\sigma}} a_{L\sigma}^\dagger a_{R\bar{\sigma}} + h.c.)$  and the Coulomb term  $H_C = \frac{1}{2} U \sum_{j,\sigma} n_{j\sigma} n_{j\bar{\sigma}}$ , with  $n_{j\sigma} \equiv a_{j,\sigma}^\dagger a_{j,\sigma}$ , the on-site energy  $\varepsilon_{L/R} = \pm \varepsilon/2$ , the charging energy  $U$ , and the spin-dependent tunneling coefficients  $t_{\sigma\sigma}$  and  $t_{\sigma\bar{\sigma}}$ . We further can show that the tunneling coefficients are inter-related by  $\vartheta$  and the *relative* SOI strength  $\gamma_{\text{so}} \equiv 2d/x_{\text{so}}$ ,

$$\begin{aligned} t_{\downarrow\downarrow} &= t_{\uparrow\uparrow}^* = t_0 (\cos \gamma_{\text{so}} - i \sin \gamma_{\text{so}} \cos \vartheta) && \equiv t, \\ t_{\downarrow\uparrow} &= t_{\uparrow\downarrow} = t_0 (-i \sin \gamma_{\text{so}} \sin \vartheta) && \equiv s, \end{aligned} \quad (2)$$

with detailed derivations in the supplementary. Here the spin-conserved ( $t$ ) and spin-flipped ( $s$ ) tunneling coefficients

are expressed in terms of  $t_0 = \sqrt{|t|^2 + |s|^2}$ , a common factor that only depends on the interdot spacing  $d$ , potential detuning  $\varepsilon$  and the barrier height  $V_0$ .

The quantum computational basis comprises the two-electron states  $\{|\uparrow\uparrow\rangle, |\uparrow\downarrow\rangle, |\downarrow\uparrow\rangle, |\downarrow\downarrow\rangle\}$ , which are the anti-symmetric, half-filling combinations of the single-electron basis states. Higher-energy two-electron states  $|S(2,0)\rangle$  and  $|S(0,2)\rangle$  have non-trivial influence on the  $(1,1)$  subspace through virtual tunneling. Their effects can be kept to  $O((t_0/U)^4)$  via a transformation. Combining Eq. (2), we can eventually deduce the effective Hamiltonian for our spin-orbit coupled DQD system as,

$$H = H_0 - J |\xi\rangle \langle \xi|. \quad (3)$$

Here  $H_0 \hat{=} \text{diag}(\varepsilon_Z, \frac{1}{2}\delta\varepsilon_Z, -\frac{1}{2}\delta\varepsilon_Z, -\varepsilon_Z)$ , with the average and difference Zeeman energy  $\varepsilon_Z \equiv (\varepsilon_{Z,L} + \varepsilon_{Z,R})/2$  and  $\delta\varepsilon_Z \equiv \varepsilon_{Z,L} - \varepsilon_{Z,R}$ . The coupling part is specified by the exchange energy  $J \equiv 2t_0^2(\frac{1}{U-\varepsilon} + \frac{1}{U+\varepsilon})$  and an entangled state

$$|\xi\rangle \equiv (s^* |\uparrow\uparrow\rangle + t^* |\uparrow\downarrow\rangle - t |\downarrow\uparrow\rangle + s |\downarrow\downarrow\rangle) / (t_0 \sqrt{2}), \quad (4)$$

or alternately  $|\xi\rangle \propto |\uparrow\rangle |\nearrow\rangle - |\downarrow\rangle |\swarrow\rangle$  by introducing a pair of “precessed” states  $|\nearrow\rangle$  and  $|\swarrow\rangle$  from the above.

To verify that Eq. (3) indeed gives rise to the anisotropic exchange coupling, we expand under the Pauli basis,  $H = \mathbf{S}_L \cdot \mathbf{B}_L + \mathbf{S}_R \cdot \mathbf{B}_R + \mathbf{S}_L \mathcal{J} \mathbf{S}_R$ , with the local spin operators  $\mathbf{S}_{L/R}$ , effective magnetic fields  $\mathbf{B}_{L/R}$  and the exchange tensor  $\mathcal{J}$ . In absence of SOI,  $\mathcal{J}$  is just a scalar, recovering the Heisenberg exchange. With nontrivial SOI,  $\mathcal{J}$  turns anisotropic. Performing spherical tensor decomposition,  $\mathbf{S}_L \mathcal{J} \mathbf{S}_R = J_0 \mathbf{S}_L \cdot \mathbf{S}_R + \mathbf{D} \cdot \mathbf{S}_L \times \mathbf{S}_R + \mathbf{S}_L \Gamma \mathbf{S}_R$ , we find the isotropic exchange energy  $J_0 = J \cos 2\gamma_{\text{so}}$ , the so-called Dzyaloshinskii-Moriya vector  $\mathbf{D} = J \sin 2\gamma_{\text{so}} \hat{\mathbf{v}}$  and the dyad  $\Gamma = J 2 \sin^2 \gamma_{\text{so}} \hat{\mathbf{v}} \hat{\mathbf{v}}$ , for  $\hat{\mathbf{v}} \equiv (-\sin \vartheta, 0, \cos \vartheta)$ . These expressions are consistent with literatures on anisotropic exchange (e.g., Ref. 18). Reversely, one can also derive Eq. (3) from these expressions. It is quite remarkable that just a single state  $|\xi\rangle$  encodes all information required for the dynamics.

We are now well-poised to study the time-evolution of qubit pairs. Before delving into details, we note that all quantum gates are understood in the rotating frame defined by the Hamiltonian  $H_0$  associated with the qubit energies [16]. For  $H = H_0 + H_I$ , the rotating-frame Hamiltonian  $e^{iH_0\tau} H_I e^{-iH_0\tau}$  generates the gate  $\tilde{U}(\tau)$ , solvable in principle with a Dyson series, or by reverse-rotation  $\tilde{U}(\tau) = e^{iH_0\tau} e^{-i(H_0+H_I)\tau}$ . In general, dramatic simplification is required for studying properties of  $\tilde{U}(\tau)$ , which is luckily possible for Eq. (3).

Our first and foremost case study is the CPhase gate, which applies a conditional  $\varphi$ -phase shift to the target qubit. A notable member is the controlled-Z (CZ) gate, a universal TQG defined at  $\varphi = \pi$ . First proposed in Ref. 15 for systems without SOI, the DC implementation of CZ has become the *de facto* way to perform TQGs in

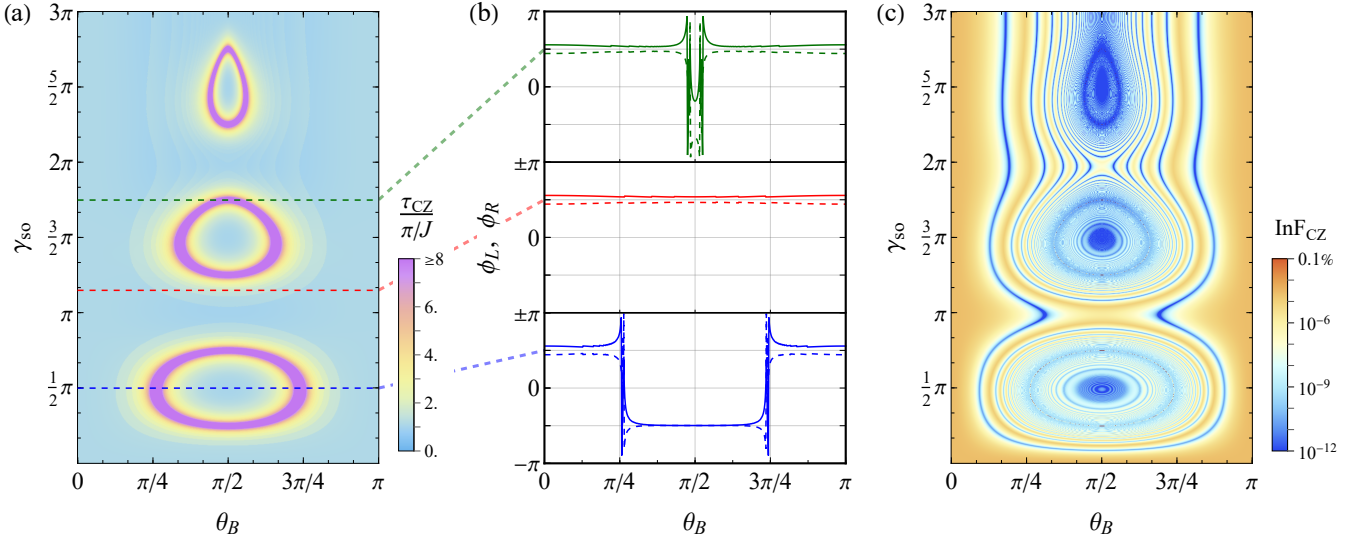


FIG. 2. Parameters of the CZ gate under SOI as functions of the magnetic field angle  $\theta_B$  and SOI strength  $\gamma_{SO}$ , plotted for a system with  $\delta E_Z/E_Z = 0.1$ ,  $J/E_Z = 0.02$  and  $d/x_0 = 3$ . (a) Gate time  $\tau_{CZ}$  in unit of  $\pi/J$ . The divergent  $\tau_{CZ}$  values are truncated at  $8\pi/J$ , which corresponds to the area with oscillatory local phase corrections. (b) Local phases  $\phi_L$  (solid line) and  $\phi_R$  (dashed line) plotted along the horizontal line cuts in (a), as indicated by their colors and vertical arrangements. (c) Gate infidelity  $\text{InF}_{CZ}$  in log scale. The case with no SOI corresponds to the  $\gamma_{SO} = 0$  line.

state-of-the-art systems [37–39]. Given its importance, here we focus on the CZ gate for brevity and our results can be directly extended to the general CPhase.

Practical implementations allow any gate that differs from the standard  $\text{CZ} \hat{=} \text{diag}(1, 1, 1, -1)$  by local phase gates [15, 37]. The local phase freedom is justified in that  $Z$ -axis rotations are “virtual” and need not be actually performed [40]. Despite this apparent freedom, here we point out that *knowledge* of the local phases is still important, e.g., at the circuit compilation step, for they could affect final measurement outcomes. We introduce the CZ-class:  $\text{CZ}[\phi] = e^{i\phi_0} Z_{\phi_L} \otimes Z_{\phi_R} \text{CZ}$ , where  $\phi_0$  is any global phase,  $\phi_{L/R}$  is the phase correction required for the left/right qubit. The gate time  $\tau_{CZ}$  is recognized as the duration  $\tau$  (in the first period) minimizing the trace distance between  $\tilde{U}(\tau)$  and  $\text{CZ}[\phi]$ , which also defines the optimal  $\phi = (\phi_0, \phi_L, \phi_R)$ . Provided  $\varepsilon_Z \gg J$ , the CZ gate is attainable with high fidelity with proper duration and phase corrections. Analytically, one can view the Hamiltonian  $H = H_0 - J|\xi\rangle\langle\xi|$  as  $H_0$  perturbed by a small coupling term. The perturbed eigenstates and eigenenergies can be used to determine  $\text{diag } \tilde{U}(\tau)$  with good accuracy. Matching up its diagonal elements with  $\text{CZ}[\phi]$ , we find  $\tilde{U}(\tau)$  approaching the target manifold when  $\tau$  becomes odd multiple of

$$\tau_{CZ} = (\pi/J)/||t/t_0|^2 - |s/t_0|^2|, \quad (5)$$

recovering  $\tau_{CZ} = \pi/J$  when  $\gamma_{SO} = 0$ . The required phase corrections  $\phi_{L/R}$  can be estimated by eigenenergy perturbations. The phase-corrected map is then compared with CZ in terms of the gate infidelity  $\text{InF}_{CZ}$ . The sec-

ond order perturbative expressions for  $\phi_{L/R}$  and  $\text{InF}_{CZ}$  can be found in the supplementary and agree well with the numerical optimization outcomes. Here, we visualize the numerical results in Fig. 2 against the control and design parameters  $\theta_B$  and  $\gamma_{SO}$  under the settings of  $\delta E_Z/E_Z = 0.1$ ,  $J/E_Z = 0.02$  and  $d/x_0 = 3$ . Fig. 2(a) gives the gate time  $\tau_{CZ}$ , in which one finds a series of divergent rings over a relatively flat base around  $\pi/J$ . According to Eq. (5), the divergent condition  $|t| = |s|$  are cases where the parallel and antiparallel spin states become symmetric, thus a phase difference is unable to accumulate. The finite ring width is due to truncation at  $8\pi/J$ , such that the ring area indicates condition where the CZ gate cannot be robustly carried out. To demonstrate this, we take three constant  $\gamma_{SO}$  lines and plot  $\phi_{L/R}$  along these lines in Fig. 2(b). The local phases vary slowly near  $\pm\pi/2$  outside and inside the rings, but change rapidly right on the rings. The gate infidelity  $\text{InF}_{CZ}$  at  $\tau_{CZ}$  and optimal  $\phi_{L/R}$  is plotted in Fig. 2(c). The most striking feature is that the infidelity inside the rings turns out to be much *lower* than that outside the rings, indicating that the gate quality could be improved by SOI. Indeed, it can be shown that the SOI “nodes” at  $\theta_B = \pi/2$  and  $\gamma_{SO} = (2k-1)\pi/2$ , ( $k = 1, 2, \dots$ ), i.e., centers of the divergent rings, are local minima of the gate infidelity function derived perturbatively. To properly characterize such improvement, we compare,

$$\begin{aligned} \text{InF}_{CZ}(\gamma_{SO} = 0) &\lesssim \frac{2}{5}(J/\delta E_Z)^2, \\ \text{InF}_{CZ}(\gamma_{SO} = \pi/2) &\lesssim \frac{1}{10}(J/E_Z)^2 \exp[\pi^2/8(d/x_0)^2]. \end{aligned} \quad (6)$$

The implications of Eq. (6) are immediate. On one hand,

to achieve high fidelity gate in system with negligible SOI, a large interdot difference in the qubit energy is required. Thus, in a system with a small  $g$ -factor variation, device design involving large magnetic field gradient  $\delta E_Z$  is a theoretical necessity rather than a technical choice. On the other hand, large magnetic field gradient is optional for quantum dots made in a semiconductor nanostructure with large SOI. The fidelity sweet-spot can be attained in systems where the dot geometry matches the SOI strength. In particular,  $4d = \pi x_{\text{SO}}$  for the first node, a condition within reach for practical systems with  $x_{\text{SO}}$  in the order of 100nm [41].

Looking beyond the CPhase gate, other novel two-qubit dynamics is also enabled after adding the SOI ingredient. Here we briefly discuss two such possibilities—the two-qubit reflection gate and the CNOT gate.

It is well-known that evolving the Heisenberg exchange Hamiltonian for  $\tau = \pi/J$  [2] produces the SWAP gate, which induces  $|\varphi\rangle|\psi\rangle \rightarrow |\psi\rangle|\varphi\rangle$  for all single-qubit states  $|\varphi\rangle$  and  $|\psi\rangle$ . Here, evolving the anisotropic exchange Hamiltonian  $H_{\text{ex}} = -J|\xi\rangle\langle\xi|$  leads to  $e^{-i(\pi/J)H_{\text{ex}}} = \mathbb{I} - 2|\xi\rangle\langle\xi|$ , i.e., a reflection of the two-qubit Hilbert space with respect to  $|\xi\rangle$ . The reflection gate generalizes over the SWAP gate, which can be seen as the reflection with respect to the Bell state  $|\Psi^-\rangle = \frac{1}{\sqrt{2}}(|\uparrow\downarrow\rangle - |\downarrow\uparrow\rangle)$ . The reflection gate recovers the SWAP gate for  $\gamma_{\text{SO}} = 0$ , but offers more general transformations with finite SOI, as the reflection state  $|\xi\rangle$  can be artificially designed by adjusting the magnetic field angle and effective SOI strength. A high-fidelity implementation of the reflection gate is achievable at the large coupling limit  $J \gg \varepsilon_Z$ —the opposite to the controlled phase gates.

A more interesting example is the DC implementation of the CNOT gate. Conventionally, the CNOT gate can be implemented in the AC way, i.e., by applying a resonant microwave drive [42]. DC implementation uses exchange interaction only and is typically less susceptible to charge noise. It would be impossible to attain the CNOT gate by a single-step evolution without SOI, as can be proven by showing the commutator  $[\text{CNOT}, H(\gamma_{\text{SO}} = 0)] \neq 0$ . When SOI is present, however, the CNOT gate can be achieved under appropriate conditions. Let us use the rotated basis  $\{|\uparrow\uparrow\rangle, |\uparrow\downarrow\rangle, |\downarrow\uparrow\rangle, |\downarrow\downarrow\rangle\}$  for convenience. At the Zeeman splitting condition  $E_{Z,L} = 3E_{Z,R}$ , the Hamiltonian (3) becomes

$$H_0 - J|\xi\rangle\langle\xi| \hat{=} \begin{pmatrix} \varepsilon_Z & 0 & 0 & 0 \\ 0 & \varepsilon_Z & 0 & 0 \\ 0 & 0 & \varepsilon_Z & 0 \\ 0 & 0 & 0 & \varepsilon_Z \end{pmatrix} - \begin{pmatrix} \frac{J}{2} & 0 & 0 & \frac{J}{2} \\ 0 & 0 & 0 & 0 \\ 0 & 0 & 0 & 0 \\ \frac{J}{2} & 0 & 0 & \frac{J}{2} \end{pmatrix}. \quad (7)$$

The representation of CNOT is in general not diagonal in this basis. But if the effective SOI strength is fixed at  $\gamma_{\text{SO}} = \pi/2$ , we have  $\text{C}_1\text{NOT}_2 \hat{=} \text{diag}(1, 1, 1, -1)$  when  $\vartheta = \pi/4$  and  $\text{C}_2\text{NOT}_1 \hat{=} \text{diag}(-1, 1, 1, 1)$  when  $\vartheta = 3\pi/4$ ,

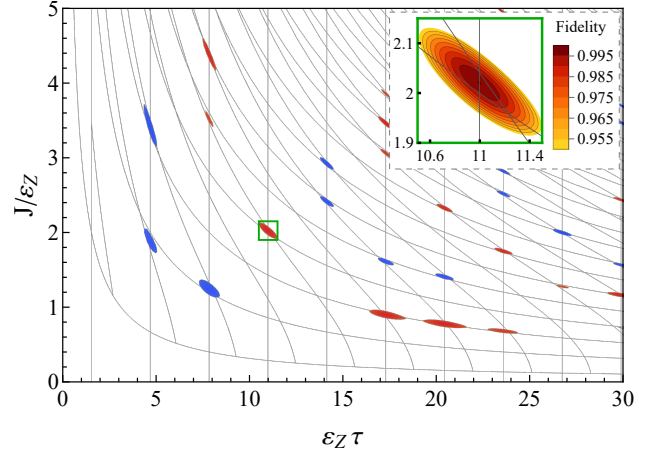


FIG. 3. Numerically computed high fidelity ( $> 95\%$ ) regions of the two-qubit CNOT gate (blue for  $\text{C}_2\text{NOT}_1$  and red for  $\text{C}_1\text{NOT}_2$ ) through DC evolution and conditions described in Eq. (8) (grey lines). The inset shows a zoom-in area where the gate fidelity values are explicitly given.

where the subscripts for C and NOT represent the control and target qubit. In both cases, they transform trivially in the rotating frame defined by  $H_0$ . Equating the interaction picture evolution  $\tilde{U}(\tau) = e^{iH_0\tau}e^{-iH\tau}$  to either CNOT gates, we obtain three independent energy-time constraints:

$$\begin{aligned} J\tau &= (2l+1)\pi, & 2\varepsilon_Z\tau &= (2m+1)\pi, \\ \sqrt{4\varepsilon_Z^2 + J^2}\tau &= 2n\pi, & \text{where } l, m, n &\in \mathbb{N}. \end{aligned} \quad (8)$$

These three conditions cannot hold simultaneously, since there is no Pythagorean triple satisfying  $(2l+1)^2 + (2m+1)^2 = (2n)^2$  [43]. But it suffices to achieve a high-fidelity gate provided that these conditions hold *approximately*. In Fig. 3, we numerically compute the gate fidelity of the  $\text{C}_1\text{NOT}_2$  and  $\text{C}_2\text{NOT}_1$  as a function of the dimensionless exchange energy  $J/\varepsilon_Z$  and evolution time  $\varepsilon_Z\tau$  (in units determined by the qubit energy  $\varepsilon_Z$ ). One can see that the high-fidelity regions appear precisely at the approximate intersections of the constraints in Eqs. (8). Through a suitable combination of the effective SOI strength  $\gamma_{\text{SO}}$ , the magnetic field angle  $\theta_B$ , the exchange energy  $J$  and evolution time  $\tau$ , one can implement the CNOT gate with fidelity surpassing 99.5% by just a single-step evolution.

In summary, we have studied the role of SOI in the dynamics of a spin qubit pair. For an exchange-coupled two-electron spin system, the compact computational Hamiltonian of Eq. (3) is derived and the connection of SOI to the anisotropic exchange interaction is revealed. Using this Hamiltonian, we deliver the central message that SOI needs not be treated as a noise source in TQGs, but rather can be naturally taken as advantages. Specifically, it is shown that the CPhase gate can be accurately implemented with adaption of SOI, and the gate fidelity



is optimized at certain practically attainable SOI nodes. It is also shown that SOI enable two-qubit dynamics that are conventionally impossible, with the general reflection gate and the CNOT gate examples explicitly constructed. Finally, we must point out that the dynamics considered here is purely unitary and errors involved are coherent in nature. This simple model should serve to demonstrate the power of SOI for facilitating high-fidelity gates and for creating novel possibilities in constructing spin-based quantum computing chips.

This work is supported by the Beijing Postdoctoral Research Foundation (Grant No. 2023-zz-050), the National Natural Science Foundation of China (Grant Nos. 92165208 and 11874071) and the Key-Area Research and Development Program of Guangdong Province (Grant No. 2020B0303060001). We would like to thank Ji-Yin Wang and Yi Luo for helpful discussions.

---

\* [qija@baqis.ac.cn](mailto:qija@baqis.ac.cn)

† [liuzh@baqis.ac.cn](mailto:liuzh@baqis.ac.cn)

‡ [hqxu@pku.edu.cn](mailto:hqxu@pku.edu.cn)

- [1] F. P. García de Arquer, D. V. Talapin, V. I. Klimov, Y. Arakawa, M. Bayer, and E. H. Sargent, *Science* **373**, eaaz8541 (2021).
- [2] D. Loss and D. P. DiVincenzo, *Physical Review A* **57**, 120 (1998).
- [3] J. W. G. van den Berg, S. Nadj-Perge, V. S. Pribiag, S. R. Plissard, E. P. A. M. Bakkers, S. M. Frolov, and L. P. Kouwenhoven, *Physical Review Letters* **110**, 066806 (2013).
- [4] J. Yoneda, K. Takeda, T. Otsuka, T. Nakajima, M. R. Delbecq, G. Allison, T. Honda, T. Kodera, S. Oda, Y. Hoshi, N. Usami, K. M. Itoh, and S. Tarucha, *Nature Nanotechnology* **13**, 102 (2018).
- [5] F. N. M. Froning, L. C. Camenzind, O. A. H. van der Molen, A. Li, E. P. A. M. Bakkers, D. M. Zumbühl, and F. R. Braakman, *Nature Nanotechnology* **16**, 308 (2021).
- [6] A.R. Mills, C.R. Guinn, M.M. Feldman, A.J. Sigillito, M.J. Gullans, M.T. Rakher, J. Kerckhoff, C.A.C. Jackson, and J.R. Petta, *Physical Review Applied* **18**, 064028 (2022).
- [7] Y. K. Kato, R. C. Myers, A. C. Gossard, and D. D. Awschalom, *Science* **306**, 1910 (2004).
- [8] S. D. Sarma, *Rev. Mod. Phys.* **76**, 88 (2004).
- [9] J. D. Sau, R. M. Lutchyn, S. Tewari, and S. Das Sarma, *Physical Review Letters* **104**, 040502 (2010).
- [10] Y. Oreg, G. Refael, and F. von Oppen, *Physical Review Letters* **105**, 177002 (2010).
- [11] V. Mourik, K. Zuo, S. M. Frolov, S. R. Plissard, E. P. A. M. Bakkers, and L. P. Kouwenhoven, *Science* **336**, 1003 (2012).
- [12] M. T. Deng, C. L. Yu, G. Y. Huang, M. Larsson, P. Caroff, and H. Q. Xu, *Nano Letters* **12**, 6414 (2012).
- [13] V. N. Golovach, M. Borhani, and D. Loss, *Physical Review B* **74**, 165319 (2006).
- [14] R. Li, J. Q. You, C. P. Sun, and F. Nori, *Physical Review Letters* **111**, 086805 (2013).
- [15] T. Meunier, V. E. Calado, and L. M. K. Vandersypen, *Physical Review B* **83**, 121403(R) (2011).
- [16] M. Russ, D. M. Zajac, A. J. Sigillito, F. Borjans, J. M. Taylor, J. R. Petta, and G. Burkard, *Physical Review B* **97**, 085421 (2018).
- [17] K. V. Kavokin, *Physical Review B* **64**, 075305 (2001).
- [18] K. V. Kavokin, *Physical Review B* **69**, 075302 (2004).
- [19] D. Stepanenko, N. E. Bonesteel, D. P. DiVincenzo, G. Burkard, and D. Loss, *Physical Review B* **68**, 115306 (2003).
- [20] F. Baruffa, P. Stano, and J. Fabian, *Physical Review Letters* **104**, 126401 (2010); *Physical Review B* **82**, 045311 (2010).
- [21] R. Li and J. Q. You, *Physical Review B* **90**, 035303 (2014).
- [22] E. Knill, R. Laflamme, and W. H. Zurek, *Proceedings of the Royal Society of London. Series A: Mathematical, Physical and Engineering Sciences* **454**, 365 (1998).
- [23] D. Aharonov and M. Ben-Or, *SIAM Journal on Computing* **38**, 1207 (2008).
- [24] X. Xue, M. Russ, N. Samkharadze, B. Undseth, A. Sammak, G. Scappucci, and L. M. K. Vandersypen, *Nature* **601**, 343 (2022).
- [25] N. E. Bonesteel, D. Stepanenko, and D. P. DiVincenzo, *Physical Review Letters* **87**, 207901 (2001).
- [26] G. Burkard and D. Loss, *Physical Review Letters* **88**, 047903 (2002).
- [27] X. Hao and S. Zhu, *Physical Review A* **76**, 044306 (2007).
- [28] G.-F. Zhang and Y. Zhou, *Physics Letters A* **370**, 136 (2007).
- [29] X. Hao and S. Zhu, *Physics Letters A* **372**, 1119 (2008).
- [30] R. J. Guerrero and F. Rojas, *Physical Review A* **77**, 012331 (2008).
- [31] Y. Zhou and G.-F. Zhang, *Optics Communications* **316**, 22 (2014).
- [32] L.-A. Wu and D. A. Lidar, *Physical Review A* **66**, 062314 (2002).
- [33] D. Stepanenko and N. E. Bonesteel, *Physical Review Letters* **93**, 140501 (2004).
- [34] C. Flindt, A. S. Sørensen, and K. Flensberg, *Physical Review Letters* **97**, 240501 (2006).
- [35] M. Milivojević and D. Stepanenko, *Journal of Physics: Condensed Matter* **29**, 405302 (2017); M. Milivojević, *Journal of Physics: Condensed Matter* **30**, 085302 (2018).
- [36] Z.-H. Liu, O. Entin-Wohlman, A. Aharony, and J. Q. You, *Physical Review B* **98**, 241303(R) (2018).
- [37] M. Veldhorst, C. H. Yang, J. C. C. Hwang, W. Huang, J. P. Dehollain, J. T. Muhonen, S. Simmons, A. Laucht, F. E. Hudson, K. M. Itoh, A. Morello, and A. S. Dzurak, *Nature* **526**, 410 (2015).
- [38] T. F. Watson, S. G. J. Philips, E. Kawakami, D. R. Ward, P. Scarlino, M. Veldhorst, D. E. Savage, M. G. Lagally, M. Friesen, S. N. Coppersmith, M. A. Eriksson, and L. M. K. Vandersypen, *Nature* **555**, 633 (2018).
- [39] K. Takeda, A. Noiri, T. Nakajima, T. Kobayashi, and S. Tarucha, *Nature* **608**, 682 (2022).
- [40] L. M. K. Vandersypen, *Rev. Mod. Phys.* **76**, 33 (2004).
- [41] J.-Y. Wang, G.-Y. Huang, S. Huang, J. Xue, D. Pan, J. Zhao, and H. Xu, *Nano Letters* **18**, 4741 (2018).
- [42] D. M. Zajac, A. J. Sigillito, M. Russ, F. Borjans, J. M. Taylor, G. Burkard, and J. R. Petta, *Science* **359**, 439 (2018).
- [43] J. H. Silverman, *A Friendly Introduction to Number Theory*, 4th ed. (Pearson, Boston, 2012) Chap. 2.

# Supplementary for Spin-Orbit Interaction Enabled High-Fidelity Two-Qubit Gates

Jiaan Qi,<sup>1,\*</sup> Zhi-Hai Liu,<sup>1,†</sup> and H. Q. Xu<sup>1,2,‡</sup>

<sup>1</sup>Beijing Academy of Quantum Information Sciences, Beijing 100193, China

<sup>2</sup>Beijing Key Laboratory of Quantum Devices, Key Laboratory for the Physics and Chemistry of Nanodevices, and School of Electronics, Peking University, Beijing 100871, China

(Dated: September 8, 2023)

## I. DERIVING THE EFFECTIVE HAMILTONIAN

Our physical set up is a double-quantum-dot (DQD) system defined in a semiconductor with strong spin-orbit interaction (SOI), containing two low-energy electrons only. The total Hamiltonian is a sum of the single-electron Hamiltonian and electron-electron interaction Hamiltonian,

$$H_{\text{tot}} = \sum_{i=1,2} H_e(\mathbf{r}_i) + \frac{e^2}{4\pi\epsilon_e|\mathbf{r}_1 - \mathbf{r}_2|}, \quad (1)$$

where  $\epsilon_e$  is the electric permittivity. Under the effective mass approximation,  $H_e$  consists of

$$H_e(\mathbf{r}) = \frac{\mathbf{p}^2}{2m_e^*} + V(\mathbf{r}) + H_{\text{so}} + H_Z, \quad (2)$$

where  $H_{\text{so}}$  is the SOI Hamiltonian and  $H_Z$  is the Zeeman Hamiltonian. The momentum operator is given by  $\mathbf{p} = -i\hbar\nabla + e\mathbf{A}$  under the magnetic field  $\mathbf{B}(\mathbf{r}) = \nabla \times \mathbf{A}$ . We leave out the optional rf electric field term here as it is irrelevant for our direct-current (DC) two-qubit-gate (TQG) implementations.

The SOI in a semiconductor can in general consists of the Rashba and Dresselhaus terms. The forms of interaction are normally defined in the crystallographic frame. By choosing  $\hat{\mathbf{x}}' \parallel [100]$ ,  $\hat{\mathbf{y}}' \parallel [010]$  and  $\hat{\mathbf{z}}'$ -axis  $\parallel [001]$ , and assuming that the electron motion is restricted in the  $\hat{\mathbf{z}}'$  direction, we have,

$$H_{\text{so}} = \alpha_R (p_{x'}\sigma_{y'} - p_{y'}\sigma_{x'}) + \alpha_D (p_{x'}\sigma_{x'} - p_{y'}\sigma_{y'}), \quad (3)$$

where  $\alpha_R$  and  $\alpha_D$  are the coupling strengths for the Rashba and Dresselhaus terms, respectively. For our DQD system, we assume that the electron motion is restricted to one dimension along a direction line that connects the two quantum dots fabricated in the (001) plane. This defines the “device frame” ( $\hat{\mathbf{x}}, \hat{\mathbf{y}}, \hat{\mathbf{z}}$ ), where the quantum dots are lining along the  $\hat{\mathbf{x}}$  axis and  $\hat{\mathbf{z}} \parallel \hat{\mathbf{z}}'$ . Denoting the angle between  $\hat{\mathbf{x}}$  and  $\hat{\mathbf{x}}'$  as  $\varphi$ , we can derive, for our DQD system with the electron motion being restricted

along the  $\hat{\mathbf{x}}$  direction, that

$$\begin{aligned} H_{\text{so}} &= p_x (\alpha_R \sigma_y + \alpha_D \cos 2\varphi \sigma_x - \alpha_D \sin 2\varphi \sigma_y) \\ &= p_x (\alpha \hat{\mathbf{c}} \cdot \boldsymbol{\sigma}) = \alpha p_x \sigma_c, \end{aligned} \quad (4)$$

where  $\hat{\mathbf{c}} \equiv \alpha^{-1}(\alpha_D \cos 2\varphi \hat{\mathbf{x}} + (\alpha_R - \alpha_D \sin 2\varphi)\hat{\mathbf{y}})$  is a unit vector representing the direction of SOI and  $\alpha$  is the normalization constant representing the strength of SOI. The restriction to one-dimension also suppresses cyclotron movement of electrons and we can neglect the gauge field as well.

Despite restriction in electron orbital motion, the electron spin can still point to all directions. The spin is understood in the “spin frame” of ( $\hat{\mathbf{a}}, \hat{\mathbf{b}}, \hat{\mathbf{c}}$ ) with spin-up/down along the  $\pm\hat{\mathbf{c}}$  direction. To eliminate the remaining uncertainty in  $\hat{\mathbf{a}}$  and  $\hat{\mathbf{b}}$ , we demand that the magnetic field  $\mathbf{B}$  lying in the upper  $\hat{\mathbf{c}}-\hat{\mathbf{a}}$  plane, such that  $\mathbf{B} \parallel \cos \theta_B \hat{\mathbf{c}} + \sin \theta_B \hat{\mathbf{a}}$  for  $\theta_B \in [0, \pi]$ , and that  $\hat{\mathbf{b}} = \hat{\mathbf{c}} \times \hat{\mathbf{a}}$ . Then we can identify

$$H_Z = \frac{1}{2} E_Z (\cos \theta_B \sigma_c + \sin \theta_B \sigma_a), \quad (5)$$

where  $E_Z \equiv g\mu_B|\mathbf{B}|$  is the Zeeman splitting energy.

The positional basis is inconvenient for studying the low energy dynamics of the system since the representation is uncountably-infinite dimensional. A much better choice is the single-electron energy eigenstates, where  $H_e$  is diagonal and we can truncate the basis to the first few terms to write down the low energy Hamiltonian. This scheme is all good except it is hard to find the exact eigenstates. Instead, another orthonormal set of electron wave function  $\{|\Phi_\mu\rangle\}$  can be used. Notice  $|\Phi_\mu\rangle$  need not be a product state of the orbital and the spin wave functions. As long as the low energy eigenstates resides in the span of the first few terms of the basis, we may truncate the basis to obtain a matrix of a finite dimension. In the field operator language, we may represent single-particle and two-particle interaction Hamiltonian by the creation  $a_\mu^\dagger$  and annihilation operator  $a_\mu$  for  $|\Phi_\mu\rangle$  as

$$H_e = \sum_{\mu\nu} T_{\mu\nu} a_\mu^\dagger a_\nu, \quad H_{ee} = \frac{1}{2} \sum_{\mu\nu\rho\lambda} V_{\mu\nu\rho\lambda} a_\mu^\dagger a_\nu^\dagger a_\rho a_\lambda. \quad (6)$$

where the coefficients are given by  $T_{\mu\nu} = \langle \Phi_\mu | H_e | \Phi_\nu \rangle$  and  $V_{\mu\nu\rho\lambda} = \langle \Phi_\mu, \Phi_\nu | H_{ee} | \Phi_\rho, \Phi_\lambda \rangle$ . The goal now is to find an appropriate basis to support the low energy wave functions. For our DQD system, the eigenequation of  $H_e$  is hard to solve analytically. But we can construct a basis

\* qija@baqis.ac.cn

† liuzh@baqis.ac.cn

‡ hqxu@pku.edu.cn

by the “linear combination of atomic orbits” method by first solving for the wave functions for two single dots and then linearly combining the two local dot wave functions to form a DQD basis.

### A. The single-dot problem

Suppose we have a single dot subject to harmonic local potential at the center of the coordinate system. Its static Hamiltonian can be written as

$$H_{\text{sd}} = \frac{p^2}{2m_e^*} + \frac{1}{2}m_e^*\Omega^2x^2 + H_{\text{so}} + H_Z \quad (7)$$

Even for such simple potential profile, analytical solutions cannot be found in a closed form. Writing down its eigenenergies and eigenstates would still require perturbation theory. Formal treatment of such Hamiltonian can be found in, e.g., Ref. 1 and Ref. 2. We briefly summarize the latter approach here, which uses the Zeeman term as perturbation, allowing treatment of strong SOI.

First, we define the unperturbed Hamiltonian  $H_0$  as the  $H_{\text{sd}}$  in Eq. (7) excluding  $H_Z$ . Conjugating  $H_0$  with  $e^{i(x/x_{\text{so}})\sigma_c}$  yields, up to a constant, the simple harmonic oscillator Hamiltonian. Therefore the  $H_0$  eigenvalues and eigenstates are found to be

$$E_{n\sigma}^{(0)} = \hbar\Omega(n + \frac{1}{2}) - \frac{1}{2}m_e^*\alpha^2, \quad (8)$$

$$|\phi_{n\sigma}^{(0)}\rangle = e^{-is_\sigma x/x_{\text{so}}} |n\rangle |\sigma\rangle \text{ with } \sigma \in \{\uparrow, \downarrow\}, \quad (9)$$

where  $x_{\text{so}} \equiv \hbar/m_e^*\alpha$  is the spin-orbit length,  $|n\rangle$  is the  $n$ th harmonic oscillator eigenstate, and  $s_{\uparrow\downarrow} = \pm 1$  is the spin-sign function. It is seen that for  $H_0$ , states with same orbital number  $n$  and opposite spins are degenerate. This degeneracy is lifted by turning on  $H_Z$ . The degenerate perturbation theory requires finding an appropriate basis that diagonalizes  $H_Z$ . For the orbital ground states in particular,

$$\langle 0|H_Z|0\rangle = \frac{E_Z}{2} \begin{pmatrix} \cos\theta_B & e^{-\eta_{\text{so}}^2} \sin\theta_B \\ e^{-\eta_{\text{so}}^2} \sin\theta_B & -\cos\theta_B \end{pmatrix}, \quad (10)$$

where we have introduced the SOI strength factor  $\eta_{\text{so}} \equiv x_0/x_{\text{so}}$  by comparing the Bohr radius  $x_0 \equiv \sqrt{\hbar/m_e^*\Omega}$  of the quantum dot to its SOI length  $x_{\text{so}}$ . Diagonalizing this matrix, we find the first-order energy corrections and the suitably oriented eigenstates to be

$$E_{0\sigma}^{(1)} = s_\sigma \frac{1}{2} f_{\text{so}} E_Z \equiv s_\sigma \frac{1}{2} \varepsilon_Z, \quad (11)$$

$$|\phi_{0\sigma}^{(0p)}\rangle = \cos(\frac{\vartheta}{2}) |\phi_{0\sigma}^{(0)}\rangle + s_\sigma \sin(\frac{\vartheta}{2}) |\phi_{0\bar{\sigma}}^{(0)}\rangle, \quad (12)$$

where we have defined the SOI-related factors

$$f_{\text{so}} \equiv \sqrt{\cos^2\theta_B + e^{-2\eta_{\text{so}}^2} \sin^2\theta_B}, \quad (13)$$

$$\vartheta \equiv \arccos(\cos\theta_B/f_{\text{so}}), \quad (14)$$

which account for the modifications of the Zeeman energy splitting and of the effective magnetic field angle due to the inclusion of SOI. For negligible SOI  $\eta_{\text{so}} \ll 1$ ,  $f_{\text{so}} \approx 1$  and  $\vartheta \approx \theta_B$  for all  $\mathbf{B}$  field angles  $\theta_B$ . In the very strong SOI regime,  $\eta_{\text{so}} \geq 2$  and  $f_{\text{so}} \approx \cos(\theta_B)$ , and thus the effective  $\mathbf{B}$  field angle is strongly regulated as  $\vartheta \approx 0$  for  $\theta_B < \pi/2$  and  $\vartheta \approx \pi$  for  $\theta_B > \pi/2$ , i.e., either parallel or antiparallel to the SOI vector. For an intermediate SOI strength, the behavior is between the above two limiting cases.

Further application of the non-degenerate perturbation theory in the rotated basis yields corrections from higher orbital states. Keeping terms up to the first order in  $\xi_Z \equiv E_Z/\hbar\Omega \ll 1$ , we have

$$|\phi_{0\sigma}^{(1)}\rangle = |\phi_{0\sigma}^{(0p)}\rangle + \sum_{n=1}^{\infty} \chi_n \left[ s_\sigma^n \cos(\frac{\vartheta}{2}) |\phi_{n\sigma}^{(0)}\rangle + s_\sigma^{n+1} \sin(\frac{\vartheta}{2}) |\phi_{n\bar{\sigma}}^{(0)}\rangle \right]. \quad (15)$$

Here, we have left out the normalization factor for brevity. The mixing amplitudes with higher orbital states are given by  $\chi_n = -\frac{1}{2}\xi_Z e^{-\eta_{\text{so}}^2} \sin(\theta_B) (\sqrt{2}i\eta_{\text{so}})^n / (n\sqrt{n!})$  and are suppressed gradually as the orbital level  $n$  increases. Similar calculations can be carried out for higher orbital levels as well. This eventually gives rise to a complete basis of states, each with entangled spin and orbital parts. In this basis, Eq. (7) is diagonal up to first order in  $\xi_Z$ , and its  $n=0$  subspace defines the qubit Hamiltonian  $H_Q = \frac{1}{2}\varepsilon_Z\sigma_c$ . But the electric dipole term  $\mathbf{E}(t) \cdot \mathbf{r}$  will not be diagonal due to nonzero matrix elements between neighboring orbital levels. This is the basis for the spin-orbit qubit and single qubit manipulations.

### B. A low energy DQD basis

The only thing left unspecified in the Hamiltonian Eq. (2) is the electro-static potential  $V(\mathbf{r}) = V(x)$  of the DQD system. In the vicinity of the local minima  $x = \pm d$ ,  $V(x)$  is approximately harmonic. We shift the energy reference level such that  $V(\mp d) = \pm\varepsilon/2$  and approximate the local harmonic potentials at  $x = -d$  and  $x = d$  by  $V_L$  and  $V_R$ . In general, the local harmonic frequencies could differ, but introducing different oscillator for each dot would be overcomplicated if only few lowest orbital levels are of interest. Here we bypass this issue by assuming that the dot frequencies are of a characteristic magnitude  $\Omega$ .  $V_L$  and  $V_R$  are defined by translating the common potential  $V_C = \frac{1}{2}m_e^*\Omega^2x^2$  to  $V_{L/R} = \frac{1}{2}m_e^*\Omega^2(x \pm d)^2$  and shifting the energy by  $\pm\varepsilon/2$ . The differences from the exact local Taylor expansions are absorbed by  $\Delta V_L$  and  $\Delta V_R$ , respectively, such that the total DQD potential can be split as

$$V = V_L + \Delta V_L = V_R + \Delta V_R. \quad (16)$$

Assuming that the effective interdot barrier is much greater compared to the orbital spacing and the dots are

well separated, the low energy eigenstates are mostly concentrated at the two single dots localied around  $x = \pm d$ . To capture those localized states, we consider translating a basis  $\{|\phi_{n\sigma}^C\rangle\}$  for the  $V_C$  potential to the left and right dots,

$$|\phi_{n\sigma}^L\rangle = e^{ipd} |\phi_{n\sigma}^C\rangle, \quad |\phi_{n\sigma}^R\rangle = e^{-ipd} |\phi_{n\sigma}^C\rangle. \quad (17)$$

Further assuming that  $\hbar\Omega \gg \varepsilon$  or  $E_Z$ , we can define a set of basis states  $O$ , ordered by increasing energy, by interleaving the two sets of basis states in Eq. (17).  $O$  is over-complete and orthogonalization is required to make proper basis. Formulating a systematic orthogonalization procedure is not the focus of this work. As a low energy theory, we can truncate the basis to only consider the four lowest orbital states  $O_{n=0}$ . Given this basis does not involve higher orbital states anyway, it make little sense to use the fully perturbed states in Eq. (15) either. But the degenerate perturbation required for breaking the Kramer degeneracy is necessary as it does not involve higher orbital states. We thus take the  $\xi_Z \ll 1$  limit and consider the properly rotated ground orbital states at the center using Eq. (12),

$$\begin{aligned} |\phi_{0\uparrow}^C\rangle &= \cos \frac{\vartheta}{2} e^{-ix/x_{SO}} |0\rangle|\uparrow\rangle + \sin \frac{\vartheta}{2} e^{+ix/x_{SO}} |0\rangle|\downarrow\rangle, \\ |\phi_{0\downarrow}^C\rangle &= \cos \frac{\vartheta}{2} e^{+ix/x_{SO}} |0\rangle|\downarrow\rangle - \sin \frac{\vartheta}{2} e^{-ix/x_{SO}} |0\rangle|\uparrow\rangle, \end{aligned} \quad (18)$$

where we follow the double-arrow convention to indicate entanglement in spin and orbital components, as opposed to single arrows for spin only.

To derive an orthonormal low-energy basis for the DQD system, we substitute Eq. (18) into Eq. (17) and calculate the state overlaps. States within the same dot are automatically orthonormal, since they are eigenstates of the local Hamiltonian,  $\langle\phi_{\sigma}^L|\phi_{\sigma'}^L\rangle = \langle\phi_{\sigma}^R|\phi_{\sigma'}^R\rangle = \delta_{\sigma\sigma'}$ . To calculate the interdot overlaps, we apply the vacuum expectation formula of displacement operators and find two distinct types of coefficients, i.e., the state overlaps between same spins and that between opposite spins,

$$\begin{aligned} s_d &\equiv \langle\phi_{0\downarrow}^L|\phi_{0\downarrow}^R\rangle = \langle\phi_{0\uparrow}^L|\phi_{0\uparrow}^R\rangle^* \\ &= e^{-(d/x_0)^2} (\cos \gamma_{SO} - i \sin \gamma_{SO} \cos \vartheta), \end{aligned} \quad (19)$$

$$\begin{aligned} s_x &\equiv \langle\phi_{0\downarrow}^L|\phi_{0\uparrow}^R\rangle = \langle\phi_{0\uparrow}^L|\phi_{0\downarrow}^R\rangle \\ &= e^{-(d/x_0)^2} (-i \sin \gamma_{SO} \sin \vartheta). \end{aligned} \quad (20)$$

where we introduce

$$\gamma_{SO} \equiv \frac{2d}{x_{SO}} = \frac{2d}{x_0} \eta_{SO}, \quad (21)$$

to characterize the SOI strength relative to the quantum dot size. To proceed with orthogonalization, we label the four DQD basis states as  $|\Phi_{L\downarrow}\rangle$ ,  $|\Phi_{L\uparrow}\rangle$ ,  $|\Phi_{R\downarrow}\rangle$  and  $|\Phi_{R\uparrow}\rangle$ , which are linear superpositions of the four local states,

$$\begin{aligned} |\Phi_{L\downarrow}\rangle &= c_{11}|\phi_{0\downarrow}^L\rangle + c_{12}|\phi_{0\uparrow}^L\rangle + c_{13}|\phi_{0\downarrow}^R\rangle + c_{14}|\phi_{0\uparrow}^R\rangle, \\ |\Phi_{L\uparrow}\rangle &= c_{21}|\phi_{0\downarrow}^L\rangle + c_{22}|\phi_{0\uparrow}^L\rangle + c_{23}|\phi_{0\downarrow}^R\rangle + c_{24}|\phi_{0\uparrow}^R\rangle, \\ |\Phi_{R\downarrow}\rangle &= c_{31}|\phi_{0\downarrow}^L\rangle + c_{32}|\phi_{0\uparrow}^L\rangle + c_{33}|\phi_{0\downarrow}^R\rangle + c_{34}|\phi_{0\uparrow}^R\rangle, \\ |\Phi_{R\uparrow}\rangle &= c_{41}|\phi_{0\downarrow}^L\rangle + c_{42}|\phi_{0\uparrow}^L\rangle + c_{43}|\phi_{0\downarrow}^R\rangle + c_{44}|\phi_{0\uparrow}^R\rangle. \end{aligned} \quad (22)$$

Applying the orthonormal condition for the basis states leads to a set of 10 independent equations. But there are in total 16 complex coefficients to solve. This indicates that there is a lot of freedom in choosing the basis states. For a representation that accurately depicting the low energy dynamics of the DQD system, we impose additional constraints out of locality and symmetry: The DQD basis states should capture the electron wave functions localized at a particular dot with a particular spin and should be symmetric with respect to the dot location and the spin direction. According to the locality principle, the DQD basis states should be considered as perturbations to the correspondingly local states. Here we choose the smallness factor to be  $e^{-(d/x_0)^2}$ . The premise that  $d/x_0$  is large is in fact mandatory for well localized dot states. As the normalization factors can be added afterwards, we demand that  $c_{ii} = 1$  with  $c_{ij} = O(e^{-(d/x_0)^2})$  for  $i \neq j$ . Orthogonality yields a set of 6 independent complex constraints,

$$\sum_{i,j} c_{mi}^* c_{nj} \langle\phi_i|\phi_j\rangle = 0, \quad \text{for } n \neq m, \quad (23)$$

where we have used the shorthands  $\phi_1, \phi_2, \phi_3$ , and  $\phi_4$  for  $\phi_{0\downarrow}^L, \phi_{0\uparrow}^L, \phi_{0\downarrow}^R$ , and  $\phi_{0\uparrow}^R$ , respectively. According to the symmetry principle, transposing the dot or the spin labels should leave the amplitude of the respective coefficients invariant. This produces 9 real constraints,

$$\begin{aligned} |c_{12}| &= |c_{21}| = |c_{34}| = |c_{43}|, \\ |c_{13}| &= |c_{31}| = |c_{24}| = |c_{42}|, \\ |c_{14}| &= |c_{41}| = |c_{32}| = |c_{23}|. \end{aligned} \quad (24)$$

Still out of symmetry consideration, we further demand the normalization factors to be identical, leading to 3 additional real constraints,

$$\begin{aligned} \sum_{i,j} c_{1i}^* c_{1j} \langle\phi_i|\phi_j\rangle &= \sum_{i,j} c_{2i}^* c_{2j} \langle\phi_i|\phi_j\rangle \\ &= \sum_{i,j} c_{3i}^* c_{3j} \langle\phi_i|\phi_j\rangle = \sum_{i,j} c_{4i}^* c_{4j} \langle\phi_i|\phi_j\rangle. \end{aligned} \quad (25)$$

We now have 24 real constraints for 24 real unknowns. Therefore, these coefficients can be in principle fully solved, producing a unique DQD basis that is both localized and symmetric. The exact coefficients, however, are quite involved functions of  $s_d$  and  $s_x$ . For our treatments, it suffices to keep these expressions to the leading order in  $e^{-(d/x_0)^2}$ . Therefore, we make the shift  $s_d \rightarrow \epsilon s_d$ ,  $s_x \rightarrow \epsilon s_x$  and  $c_{ij} \rightarrow \epsilon c_{ij} + \epsilon^2 d_{ij} + \dots$ ,  $i \neq j$ . Solving the constraints to the leading order, we have

$$\begin{aligned} c_{12} &= c_{21} = c_{34} = c_{43} = 0, \\ c_{13} &= c_{31}^* = c_{24}^* = c_{42} = -s_d^*/2, \\ c_{14} &= c_{41}^* = c_{23}^* = c_{32}^* = -s_x^*/2. \end{aligned} \quad (26)$$

These solutions are in fact good enough for all constraints to remain valid up to  $O(\epsilon^2)$ , Therefore we may write our



DQD basis states as

$$\begin{aligned}
|\Phi_{L\downarrow}\rangle &= |\phi_{0\downarrow}^L\rangle - \frac{1}{2}s_d^*|\phi_{0\downarrow}^R\rangle - \frac{1}{2}s_x^*|\phi_{0\uparrow}^R\rangle, \\
|\Phi_{L\uparrow}\rangle &= |\phi_{0\uparrow}^L\rangle - \frac{1}{2}s_d|\phi_{0\uparrow}^R\rangle - \frac{1}{2}s_x^*|\phi_{0\downarrow}^R\rangle, \\
|\Phi_{R\downarrow}\rangle &= |\phi_{0\downarrow}^R\rangle - \frac{1}{2}s_d|\phi_{0\downarrow}^L\rangle - \frac{1}{2}s_x|\phi_{0\uparrow}^L\rangle, \\
|\Phi_{R\uparrow}\rangle &= |\phi_{0\uparrow}^R\rangle - \frac{1}{2}s_d^*|\phi_{0\uparrow}^L\rangle - \frac{1}{2}s_x|\phi_{0\downarrow}^L\rangle.
\end{aligned} \tag{27}$$

### C. The second-quantized Hamiltonian

Equipped with the low energy basis, we proceed to derive the low energy Hamiltonian for the DQD system.

Focusing on the single-electron Hamiltonian  $H_e$ , the state indices in Eq. (6) now include both the site and spin-orbit quantum numbers:  $T_{X\sigma, X'\sigma'} = \langle \Phi_{X\sigma} | \hat{H}_e | \Phi_{X'\sigma'} \rangle$ , and there are 16 elements in total. Since the DQD basis states are linear combinations of the local dot states, these matrix elements are also linear combinations of the Hamiltonian matrix elements with respect to the local dot states,  $\tilde{T}_{X\sigma, X'\sigma'} = \langle \phi_{X\sigma} | \hat{H}_e | \phi_{X'\sigma'} \rangle$ , by

$$T_{ij} = \sum_{kl} C_{ik}^* \tilde{T}_{kl} C_{jl} = (C^* \tilde{T} C^T)_{ij}. \tag{28}$$

The basis transformation matrix is given by Eq. (27),

$$C = \begin{pmatrix} 1 & 0 & -\frac{1}{2}s_d^* & -\frac{1}{2}s_x^* \\ 0 & 1 & -\frac{1}{2}s_x^* & -\frac{1}{2}s_d \\ -\frac{1}{2}s_d & -\frac{1}{2}s_x & 1 & 0 \\ -\frac{1}{2}s_x & -\frac{1}{2}s_d^* & 0 & 1 \end{pmatrix}. \tag{29}$$

According the Eq. (16), we can decompose  $H_e = H_L + \Delta V_L = H_R + \Delta V_R$ , and calculate

$$\tilde{T} = \begin{pmatrix} \varepsilon_{L\downarrow} + v_- & 0 & s_d(\varepsilon_{R\downarrow} + v_0) & s_x(\varepsilon_{R\uparrow} + v_0) \\ 0 & \varepsilon_{L\uparrow} + v_- & s_x(\varepsilon_{R\downarrow} + v_0) & s_d^*(\varepsilon_{R\uparrow} + v_0) \\ s_d^*(\varepsilon_{R\downarrow} + v_0^*) & s_x^*(\varepsilon_{R\downarrow} + v_0^*) & \varepsilon_{R\downarrow} + v_+ & 0 \\ s_x^*(\varepsilon_{R\uparrow} + v_0^*) & s_d(\varepsilon_{R\uparrow} + v_0^*) & 0 & \varepsilon_{R\uparrow} + v_+ \end{pmatrix} \tag{30}$$

where  $\varepsilon_{L/R, \sigma} = \pm\varepsilon + s_\sigma \frac{1}{2}\varepsilon_{L/R, Z}$  is the energy of the local Hamiltonian  $H_{L/R}$ , while

$$\begin{aligned}
v_- &\equiv \langle 0 | e^{-ipd} \Delta V_L e^{ipd} | 0 \rangle = \langle 0 | \Delta V_L(x-d) | 0 \rangle, \\
v_+ &\equiv \langle 0 | e^{ipd} \Delta V_R e^{-ipd} | 0 \rangle = \langle 0 | \Delta V_R(x+d) | 0 \rangle,
\end{aligned} \tag{31}$$

are the energy corrections due to the existence of the other dot, and finally,

$$v_0 \equiv \frac{\langle 0 | e^{-ipd} \Delta V_R e^{-ipd} | 0 \rangle}{\langle 0 | e^{-2ipd} | 0 \rangle} = \langle 0 | \Delta V_R(x) | 0 \rangle, \tag{32}$$

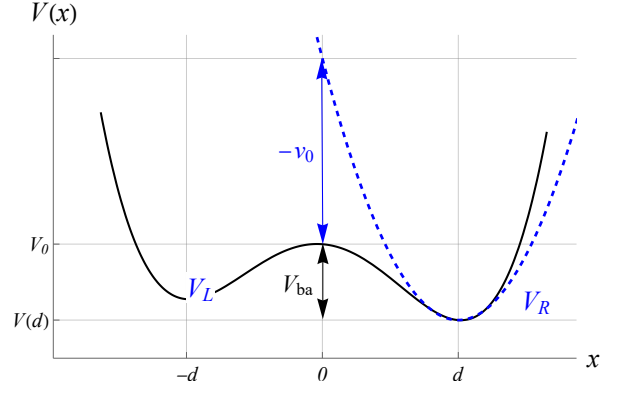


FIG. 1: The  $v_0$  term as determined by the potential profile

where we have used the Wick's theorem to simplify the vacuum expectations. Since  $\Delta V_{L/R}$  is by definition close to zero in the vicinity of  $x = \mp d$ , the values of  $v_-$  and  $v_+$  are typically much smaller than other energy scales. On the other hand,  $v_0$  is related to barrier of the DQD system. Specifically, assuming  $d \gg x_0$ , we can approximate

$$v_0 \approx V(0) - V(d) - \frac{1}{2}m_e^* \Omega^2 d^2. \tag{33}$$

As illustrated in Fig. 1, the parabolically shaped  $V_R$  will tend to overestimate the DQD potential  $V$  at  $x = 0$ . Therefore  $v_0$  is negative and its magnitude is typically much greater than other energy scales such as the orbital detuning and the Zeeman energy. Furthermore, increasing the barrier height  $V_{ba}$  will decrease  $|v_0|$ , thus decreasing the tunneling amplitude. This is consistent with typical observations.

Applying the transformation in Eq. (28) and keep the terms up to the first order of the smallness factor  $e^{-(d/x_0)^2}$ , we find,

$$T = \begin{pmatrix} \varepsilon_{L\downarrow} + v_- & 0 & t_\downarrow & s_\downarrow \\ 0 & \varepsilon_{L\uparrow} + v_- & s_\uparrow & t_\uparrow \\ t_\downarrow^* & s_\uparrow^* & \varepsilon_{R\downarrow} + v_+ & 0 \\ s_\downarrow^* & t_\uparrow^* & 0 & \varepsilon_{R\uparrow} + v_+ \end{pmatrix}, \tag{34}$$

where we introduce the tunneling coefficients

$$\begin{aligned}
t_\downarrow &= s_d \left( \frac{1}{2}\varepsilon_{R\downarrow} - \frac{1}{2}\varepsilon_{L\downarrow} + v_0 - \frac{1}{2}v_- - \frac{1}{2}v_+ \right), \\
t_\uparrow &= s_d^* \left( \frac{1}{2}\varepsilon_{R\uparrow} - \frac{1}{2}\varepsilon_{L\uparrow} + v_0 - \frac{1}{2}v_- - \frac{1}{2}v_+ \right), \\
s_\downarrow &= s_x \left( \frac{1}{2}\varepsilon_{R\uparrow} - \frac{1}{2}\varepsilon_{L\downarrow} + v_0 - \frac{1}{2}v_- - \frac{1}{2}v_+ \right), \\
s_\uparrow &= s_x \left( \frac{1}{2}\varepsilon_{R\downarrow} - \frac{1}{2}\varepsilon_{L\uparrow} + v_0 - \frac{1}{2}v_- - \frac{1}{2}v_+ \right).
\end{aligned} \tag{35}$$

The dot Hamiltonian  $H_d$  is defined according to the diagonal part of the  $T$  tensor. We may redefine the effective chemical potentials to  $\tilde{\varepsilon}_{L\sigma} = \varepsilon_{L\sigma} + v_-$  and  $\tilde{\varepsilon}_{R\sigma} = \varepsilon_{L\sigma} + v_+$ ; or, as argued earlier, simply neglect the  $v_\pm$  terms since they are very small. Since shifting the global energy level

has trivial influence on the qubit dynamics, We can reset  $\tilde{\varepsilon}_L + \tilde{\varepsilon}_R = 0$  and define detuning  $\varepsilon = \tilde{\varepsilon}_L - \tilde{\varepsilon}_R$ . by

$$\hat{H}_d = \sum_{\sigma=\uparrow,\downarrow} \frac{1}{2}(\varepsilon + s_\sigma \varepsilon_{Z,L})n_{L\sigma} + \frac{1}{2}(-\varepsilon + s_\sigma \varepsilon_{Z,R})n_{R\sigma} \quad (36)$$

The Zeeman splitting energy can be further rearranged into the average splitting  $\varepsilon_Z = (\varepsilon_{Z,L} + \varepsilon_{Z,R})/2$  and the energy difference  $\delta\varepsilon_Z = (\varepsilon_{Z,L} - \varepsilon_{Z,R})$ .

The tunneling Hamiltonian  $H_t$  is the off-diagonal part of the  $T$  tensor. In principle, there are mechanisms involved: spin-preserved and spin-flipped tunneling, in addition to on-site spin flipping. If there is no oscillatory electric field, on-site flipping term is absent and we have,

$$H_t = \sum_{\sigma=\uparrow,\downarrow} (t_\sigma a_{L\sigma}^\dagger a_{R\sigma} + s_\sigma a_{L\sigma}^\dagger a_{R\bar{\sigma}} + h.c.), \quad (37)$$

where spin-dependent tunneling coefficients are given by Eq. (35). Calculating these coefficients requires knowledge of the full potential profile, but the details of the potential contributes trivially to the the gate dynamics by  $v_0, v_-$  and  $v_+$ . In the presence of the barrier term  $v_0$ , the Zeeman energy differences in the parentheses of Eq. (35) can be safely ignored. Combining with Eq. (19), we can define a common tunneling strength  $t_0 \propto e^{-(d/x_0)^2}$  for the spin-conserved tunneling  $t$  and spin-flipped tunneling  $s$ , which are related by

$$t \equiv t_\downarrow = t_\uparrow^* = t_0 [\cos(\gamma_{so}) - i \sin(\gamma_{so}) \cos(\vartheta)], \quad (38)$$

$$s \equiv s_\downarrow = s_\uparrow = t_0 [-i \sin(\gamma_{so}) \sin(\vartheta)]. \quad (39)$$

Finally, the electron interaction energy involves in many terms and can also contribute to the exchange interaction. This is known as direct exchange and it mainly affects doubly occupied sites. This differs from the kinetic exchange that arises from  $H_t$ . Here we only consider leading order effect where all terms in the  $V$  tensor are ignored and only on-site Coulomb repulsion is considered. This can be summarized as

$$H_C = \sum_{j=L,R} \sum_{\sigma=\uparrow,\downarrow} \frac{U}{2} a_{j\sigma}^\dagger a_{j\sigma}^\dagger a_{j\bar{\sigma}} a_{j\bar{\sigma}} \quad (40)$$

#### D. Hamiltonian in the computational space

In order to derive the effective exchange Hamiltonian, we expand the system Hamiltonian in the six low energy two-electron spin basis that consists of 4 states in the (1,1) configuration and the singlet state  $S(2,0)$  and  $S(0,2)$ . Each of these basis are antisymmetric two-

electron wave functions, explicitly,

$$\begin{aligned} |\uparrow\uparrow\rangle &= \frac{1}{\sqrt{2}} (|\Phi_{L\uparrow}\rangle_1 |\Phi_{R\uparrow}\rangle_2 - |\Phi_{R\uparrow}\rangle_1 |\Phi_{L\uparrow}\rangle_2), \\ |\uparrow\downarrow\rangle &= \frac{1}{\sqrt{2}} (|\Phi_{L\uparrow}\rangle_1 |\Phi_{R\downarrow}\rangle_2 - |\Phi_{R\downarrow}\rangle_1 |\Phi_{L\uparrow}\rangle_2), \\ |\downarrow\uparrow\rangle &= \frac{1}{\sqrt{2}} (|\Phi_{L\downarrow}\rangle_1 |\Phi_{R\uparrow}\rangle_2 - |\Phi_{R\uparrow}\rangle_1 |\Phi_{L\downarrow}\rangle_2), \\ |\downarrow\downarrow\rangle &= \frac{1}{\sqrt{2}} (|\Phi_{L\downarrow}\rangle_1 |\Phi_{R\downarrow}\rangle_2 - |\Phi_{R\downarrow}\rangle_1 |\Phi_{L\downarrow}\rangle_2), \\ |S(2,0)\rangle &= \frac{1}{\sqrt{2}} (|\Phi_{L\uparrow}\rangle_1 |\Phi_{L\downarrow}\rangle_2 - |\Phi_{L\downarrow}\rangle_1 |\Phi_{L\uparrow}\rangle_2), \\ |S(0,2)\rangle &= \frac{1}{\sqrt{2}} (|\Phi_{R\uparrow}\rangle_1 |\Phi_{R\downarrow}\rangle_2 - |\Phi_{R\downarrow}\rangle_1 |\Phi_{R\uparrow}\rangle_2). \end{aligned} \quad (41)$$

The tunneling Hamiltonian, for example, acts on the  $|\downarrow\uparrow\rangle$  by

$$\begin{aligned} H_t |\downarrow\uparrow\rangle &= t_\uparrow a_{L\uparrow}^\dagger a_{R\uparrow} |\downarrow\uparrow\rangle + t_\downarrow^* a_{L\downarrow}^\dagger a_{L\downarrow} |\downarrow\uparrow\rangle \\ &= -t^* |S(2,0)\rangle - t^* |S(0,2)\rangle. \end{aligned} \quad (42)$$

Using similar calculations, we can represent the low energy Hamiltonian as

$$H_6 \cong \begin{pmatrix} \varepsilon_Z & 0 & 0 & 0 & s^* & -s \\ 0 & \frac{1}{2}\delta\varepsilon_Z & 0 & 0 & t^* & t^* \\ 0 & 0 & -\frac{1}{2}\delta\varepsilon_Z & 0 & -t & -t \\ 0 & 0 & 0 & -\varepsilon_Z & -s^* & s \\ s & t & -t^* & -s & U - \varepsilon & 0 \\ -s^* & t & -t^* & s^* & 0 & U + \varepsilon \end{pmatrix}, \quad (43)$$

under the basis  $\{|\uparrow\uparrow\rangle, |\uparrow\downarrow\rangle, |\downarrow\uparrow\rangle, |\downarrow\downarrow\rangle, |S(2,0)\rangle, |S(0,2)\rangle\}$ . Assuming that the on-site Coulomb energy is much larger than the tunneling energy:  $U \gg t_0$ , we would have three different energy blocks—(1,1), (0,2), (2,0) with weak coupling. The DC gates work exclusively in the (1,1) charge configuration. To find the influence of other energy levels on the (1,1) space, we project  $H_6$  in to four (1,1) states space using the Schrieffer-Wolff transformation  $e^S H_6 e^{-S}$ . Define the diagonal and off-diagonal part of  $H_6$  as  $H_{60}$  and  $H_{61}$ , the transformation matrix  $S$  must satisfy the condition  $[H_{60}, S] = H_{61}$ . And the effective Hamiltonian in the (1,1) charge configuration can be approximate with

$$H = \mathcal{P}_{(1,1)} \left( H_{60} + \frac{1}{2} [S, H_{61}] \right) + O((t_0/U)^4). \quad (44)$$

Since  $H_{60}$  is diagonal,  $S$  can be explicitly found by,

$$S_{ii} = 0, \quad S_{ij} = \frac{(H_{61})_{ij}}{(H_{60})_{ii} - (H_{60})_{jj}} \quad (i \neq j). \quad (45)$$

Substituting into Eq. (44), we can write the resulting effective Hamiltonian as

$$H = H_0 + H_I, \quad (46)$$

where,

$$H_0 = \begin{pmatrix} \varepsilon_Z & & & \\ & \frac{1}{2}\delta\varepsilon_Z & & \\ & & -\frac{1}{2}\delta\varepsilon_Z & \\ & & & -\varepsilon_Z \end{pmatrix}, \quad (47)$$

is a diagonal matrix that arises solely from the local Zeeman field for each dot.  $H_I$  is responsible for the exchange coupling, explicitly given by its  $(i, j)$ th element,

$$(H_I)_{ij} = -2(\mathbf{j}_i + \mathbf{j}_j)\boldsymbol{\xi}_i\boldsymbol{\xi}_j^*, \quad (48)$$

where we introduce vectors

$$\mathbf{j} = t_0^2(\alpha_-, \beta_-, \beta_+, \alpha_+)^T, \quad (49)$$

$$\boldsymbol{\xi} = 1/(\sqrt{2}t_0)(s^*, t^*, -t, s)^T, \quad (50)$$

with,

$$\alpha_{\pm} = \frac{1}{2} \left( \frac{1}{U \pm \varepsilon_Z - \varepsilon} + \frac{1}{U \pm \varepsilon_Z + \varepsilon} \right), \quad (51)$$

$$\beta_{\pm} = \frac{1}{2} \left( \frac{1}{U \pm \delta\varepsilon_Z - \varepsilon} + \frac{1}{U \pm \delta\varepsilon_Z + \varepsilon} \right).$$

Because  $U \gg \varepsilon_Z, \delta\varepsilon_Z$ , we can make the approximation

$$\alpha_{\pm} \approx \beta_{\pm} \approx \frac{1}{2} \left( \frac{1}{U - \varepsilon} + \frac{1}{U + \varepsilon} \right) \equiv \frac{J}{4t_0^2}. \quad (52)$$

Due to the form  $\boldsymbol{\xi}$  is defined, we can define normalized state  $|\xi\rangle$  whose components is given by Eq. (50). This leads to the simplified expression

$$H_1 = -J|\xi\rangle\langle\xi|. \quad (53)$$

We may alternately defined  $|\xi\rangle$  as the entangled two-qubit state

$$|\xi\rangle = \frac{1}{\sqrt{2}}(|\uparrow\rangle|\nearrow\rangle - |\downarrow\rangle|\swarrow\rangle), \quad (54)$$

where,

$$\begin{aligned} |\nearrow\rangle &= \tilde{s}^*|\uparrow\rangle + \tilde{t}^*|\downarrow\rangle, \\ |\swarrow\rangle &= \tilde{t}|\uparrow\rangle - \tilde{s}|\downarrow\rangle \end{aligned} \quad (55)$$

are a pair of orthogonal spin states with normalized coefficients  $|\tilde{s}|^2 + |\tilde{t}|^2 = 1$  given by  $\tilde{s} = s/t_0$  and  $\tilde{t} = t/t_0$ .

For operators on the two-qubit Hilbert space, a complete operator basis with respect to the Hilbert-Schmidt inner product is given by the two-qubit Pauli operators  $\{\sigma^i \otimes \sigma^j\}$ , where  $(i, j) = (0, 0), (0, 1), \dots, (3, 3)$ . For the DQD low energy Hamiltonian, the Pauli representation allows direct read-off of a standard form of the two-qubit Hamiltonian, defined by

$$H = \mathbf{S}_L \cdot \mathbf{B}_L + \mathbf{S}_R \cdot \mathbf{B}_R + \mathbf{S}_L \mathcal{J} \mathbf{S}_R, \quad (56)$$

where  $\mathbf{S}_L = \frac{1}{2}\boldsymbol{\sigma}_L$  and  $\mathbf{S}_R = \frac{1}{2}\boldsymbol{\sigma}_R$  are the spin operators for the left and right dot;  $\mathbf{B}_L$  and  $\mathbf{B}_R$  are the effective B fields and  $\mathcal{J}$  is the spin exchange tensor. As the Pauli basis is complete, this describes the most general form of two-qubit Hamiltonian. For the conventional Heisenberg exchange interaction, the exchange tensor is just a scalar, i.e., isotropic. On the other hand, anisotropic exchange interaction is also possible. The exchange Hamiltonian is in general represented as

$$\mathbf{S}_L \mathcal{J} \mathbf{S}_R = J_0 \mathbf{S}_L \cdot \mathbf{S}_R + \mathbf{D} \cdot \mathbf{S}_L \times \mathbf{S}_R + \mathbf{S}_L \Gamma \mathbf{S}_R, \quad (57)$$

where  $J_0$  is the isotropic exchange energy,  $\mathbf{D}$  is the so-called Dzyaloshinskii-Moriya (DM) vector and  $\Gamma$  is a symmetric tensor. We see that this representation is simply the spherical tensor decomposition of the exchange tensor  $\mathcal{J}$ . Expanding the Hamiltonian (52) in the Pauli operator basis, we can express the exchange tensor in terms of  $\gamma_{\text{SO}}$  and  $\vartheta$  by

$$\mathcal{J} = J \begin{pmatrix} \cos^2\gamma_{\text{SO}} - \sin^2\gamma_{\text{SO}} \cos 2\vartheta & \sin 2\gamma_{\text{SO}} \cos \vartheta & -\sin^2\gamma_{\text{SO}} \sin 2\vartheta \\ -\sin 2\gamma_{\text{SO}} \cos \vartheta & \cos 2\gamma_{\text{SO}} & -\sin 2\gamma_{\text{SO}} \sin \vartheta \\ -\sin^2\gamma_{\text{SO}} \sin 2\vartheta & \sin 2\gamma_{\text{SO}} \sin \vartheta & \cos^2\gamma_{\text{SO}} + \sin^2\gamma_{\text{SO}} \cos 2\vartheta \end{pmatrix}. \quad (58)$$

Hence we conclude that SOI will render the exchange coupling anisotropic in general. Defining a vector  $\hat{\mathbf{v}} = (-\sin \vartheta, 0, \cos \vartheta)$ , we can associate,

$$\begin{aligned} J_0 &= J \cos 2\gamma_{\text{SO}}, \\ \mathbf{D} &= J \sin 2\gamma_{\text{SO}} \hat{\mathbf{v}}, \\ \Gamma &= J 2 \sin^2\gamma_{\text{SO}} \hat{\mathbf{v}} \hat{\mathbf{v}}, \end{aligned} \quad (59)$$

for the terms in Eq. (57). On the other hand, from the same Pauli representation, we find that the effective magnetic field is not affected by the presence of SOI.

## II. DC TIME EVOLUTIONS

### A. rotating frame and local phase corrections

For two-qubit systems, the Hamiltonian  $H_0 = H_{Q_1} + H_{Q_2}$  defines the energy quantization for each qubit and needs to be deducted from the total Hamiltonian for any transformation on the qubit states. In other words, any qubit state is defined in the rotation frame by  $|\psi(t)\rangle_{\text{rf}} = R^{-1}|\psi(t)\rangle_{\text{lab}}$  with  $R(t) = e^{-iH_0 t}$ , where we assumed time-independent  $H_0$  here for brevity but our discussion can be easily applied to the time-dependent case. Splitting the total Hamiltonian into  $H = H_0 + H_1$ , the rotating frame Hamiltonian  $\tilde{H}(t) = R^{-1}(t)H_1R(t)$  is responsible for generating the two-qubit joint evolution (gate),

$$\tilde{U}(t) = \mathcal{T} \exp \left( -i \int_0^t \tilde{H}(t') dt' \right), \quad (60)$$

where  $\mathcal{T}$  is the time ordering operator. Alternatively, we can reversely rotate the lab frame time evolution operator  $U(t)$  and get

$$\tilde{U}(t) = R^{-1}(t)U(t) = e^{iH_0 t} e^{-i(H_0 + H_1)t}. \quad (61)$$

Under the assumption that  $H$  is constant within the time frame involved,  $U(t) = e^{-iHt}$  is much simpler than a Dyson series needed to express  $\tilde{U}(t)$ . In general  $e^{iH_0 t} e^{-i(H_0 + H_1)t} \neq e^{-iH_1 t}$ , particularly when  $t$  is large the LHS and RHS are not even close to each other in the sense of BCH series. Therefore specific simplifications are required to derive the rotating frame evolutions.

It is often difficult to realize the target gate directly from the time evolution. Instead, we may allow any gate that differs from the target gate by local phase gates,  $Z_\phi = e^{-i(\phi/2)\sigma_z}$ . Moreover, as is with all quantum states, there can be an arbitrary global phase factor as well. Taking these phase degrees of freedom into account, we define

$$\begin{aligned} G[\phi] &\equiv \{ e^{i\phi_0} (Z_{\phi_1} \otimes Z_{\phi_2}) G, \mid \forall \phi_0, \phi_1, \phi_2 \} \\ &= \{ \text{diag}(e^{i\phi_0}, e^{i\phi_2}, e^{i\phi_1}, e^{i\phi_3}) G, \mid \phi_0 + \phi_3 = \phi_1 + \phi_2 \}. \end{aligned} \quad (62)$$

Now the target is not a single point in the  $\text{SU}(4)$  space, but rather a three-dimensional manifold charted by the phase parameters  $\phi = (\phi_0, \phi_1, \phi_2)$ . We can establish an equivalence relations between operators in  $\text{SU}(4)$ :  $G_1 \sim G_2$  if and only if they can be connected through global and local phase corrections. In particular, we find that the rotating frame is also equivalent to a local phase correction and thus  $\tilde{U}(\tau) \sim U(\tau)$ .

To implement  $G$ , we wish that  $\tilde{U}(t)$  to be close to, if not belong to, the set  $\{G\}_\phi$  at certain time  $t_G$ . A correct definition for the distance to the target manifold is given by the optimization,

$$D(t) \equiv \min_{-\pi < \phi \leq \pi} \|\tilde{U}(t) - G[\phi]\|, \quad (63)$$

where the restriction to the  $\phi_i \in (-\pi, \pi]$  cube accounts for the  $2\pi$  periodicity of the phase factors. Having defined the instantaneous distance function  $D(t)$ , a further optimization with respect to time identifies the minimal distance and the gate time,

$$D_{\min} \equiv \min_t D(t), \quad \tau_{\text{CZ}} \equiv \arg \min_t D(t). \quad (64)$$

In Fig. 2a, we illustrate the distribution of the norm distance within the phase space  $(\phi_0, \phi_1, \phi_2)$  for a typical time evolution operator  $\tilde{U}(t)$  at a fixed time instant. There can be multiple local minimums in general, which poses some difficulty for naive numerical algorithms. In Fig. 2b, we use the stochastic differential evolution method to numerically determine the global minimal distance at each time instance, yielding a zigzag function dipped at odd multiples of  $t_{\text{CZ}}$ . Since the minimal distance  $D_{\min}$  in Fig. 2b is very small, we can conclude that the CZ gate is achieved with high accuracy by under  $\tilde{H}(t)$ .

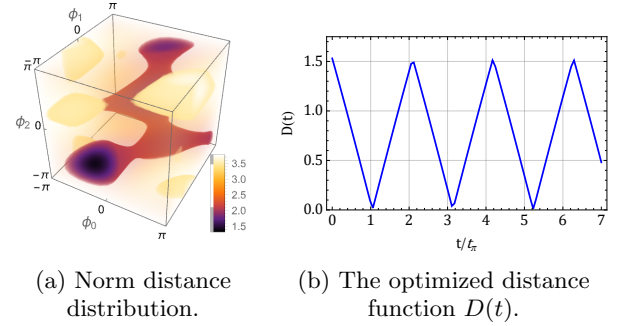


FIG. 2: The distance of  $\tilde{U}(t)$  to the CZ manifold. (a) At each instant,  $D(t)$  is defined by minimization within the phase space. (b) The  $D(t)$  function yields a minimal distance  $D_{\min}$  at  $t_{\text{CZ}} \approx 1.05\pi/J$ , where the target CZ gate is achieved.

### B. The CZ/CPHASE gate

The CZ gate is a two-qubit gate that applies a phase-flip (Z-gate) to the target qubit conditioned on the control qubit. In the standard two-qubit basis  $\{|00\rangle, |01\rangle, |10\rangle, |11\rangle\}$ , it is represented as:  $\text{CZ} = \text{diag}(1, 1, 1, -1)$ . Taking account into the local and global phase freedom, we explicitly write  $\text{CZ}[\phi]$  as

$$\begin{aligned} \text{CZ}[\phi] &= e^{i\phi_0} Z_{\phi_L} \otimes Z_{\phi_R} \text{CZ} \\ &\doteq \text{diag}(e^{i\phi_0}, e^{i(\phi_0 + \phi_R)}, e^{i(\phi_0 + \phi_L)}, -e^{i(\phi_0 + \phi_L + \phi_R)}), \end{aligned} \quad (65)$$

where  $\phi_L, \phi_R$  are local phase corrections on the left and right dot; and the dot-equal sign represents equality up to a global phase. Additional conditions that often appear in literatures are  $\phi_1 + \phi_2 = \pi$  and  $\phi_0 = 0$ , where the



phase for the parallel states vanishes and one only need to accumulate a combined phase of  $\pi$  for the anti-parallel states. To find out how successful this time evolution implement the CZ gate, we can use gate infidelity as our distance measure,

$$\text{Inf}_G = 1 - F_G = \frac{d^2 - |\text{tr}(G^\dagger \tilde{U})|^2}{d + d^2}. \quad (66)$$

In our case,  $G = \text{CZ}[\phi]$  is the target gate and the dimension  $d = 4$ . Since  $\text{CZ}[\phi]$  is diagonal, the trace product depends only on the diagonal elements.

As only the diagonal element enters the calculation, it is desirable to know the diagonal elements of the matrix  $\tilde{U}(\tau)$ . Assuming  $\varepsilon_Z \gg J$ , we can determine these diagonal elements with the help of perturbation theory. Based on our assumption, the Hamiltonian  $H = H_0 - J|\xi\rangle\langle\xi|$  can be seen as  $H_0$  perturbed by a much smaller term. Let us denote the eigenenergies of  $H_0$  as  $E_n^{(0)} \equiv \langle n|H_0|n\rangle$ , where  $|n\rangle$  is the  $n$ th computational basis state. The perturbed eigenenergies and eigenstates are

$$E'_n = E_n^{(0)} + \delta E_n, \quad (67)$$

$$|n'\rangle = \frac{1}{\sqrt{N_n}}|\tilde{n}'\rangle, \quad |\tilde{n}'\rangle = |n\rangle + |\delta n\rangle, \quad (68)$$

where  $|\tilde{n}'\rangle$  is the unnormalized eigenstate with  $\langle n|\delta n\rangle = 0$ . The normalization factor is determined by the inner product

$$N_n = \langle \tilde{n}'|\tilde{n}'\rangle = 1 + \langle \delta n|\delta n\rangle. \quad (69)$$

To calculate the diagonal elements of  $\tilde{U}(\tau) = e^{iH_0\tau}e^{-iH\tau}$ , we take the matrix exponential  $e^{-iH\tau}$  in the eigenstate basis of  $H$  and then perform projection onto the diagonal

space. Also since  $H_0$  is already diagonal, we have

$$\begin{aligned} \langle n|\tilde{U}(\tau)|n\rangle &= e^{iE_n^{(0)}\tau} \langle n|e^{-iH\tau}|n\rangle \\ &= \underbrace{\frac{1}{N_n}e^{-i\delta E_n\tau}}_{\text{major} \sim O(1)} + \sum_{m \neq n} \underbrace{\frac{|\langle n|\delta m\rangle|^2}{N_m}e^{-i(E'_m - E_n^{(0)})\tau}}_{\text{minor} \sim O((J/\varepsilon_Z)^2)}, \end{aligned} \quad (70)$$

where we have split the expression into a major part originating from the overlap  $\langle n'|n\rangle = O(1)$  and a minor part originating from  $\langle \delta m|n\rangle = O((J/\varepsilon_Z)^2)$  for  $m \neq n$ . For our goal of deriving a perturbative expression, it suffice to consider the condition where the major part implements  $\text{CZ}[\phi]$  and absorb the rest into errors. Comparing with Eq. (65), we see that the DC evolution reaches the target  $\text{CZ}[\phi]$  gate when it meet the phase-matching condition:

$$(\delta E_1 + \delta E_4 - \delta E_2 - \delta E_3)\tau = (2k + 1)\pi, \quad k \in \mathbb{Z}. \quad (71)$$

To derive an appropriate condition, we consider calculate the energy perturbation to the second order:

$$\delta E_n = -J|\langle n|\xi\rangle|^2 + \sum_{k \neq n} \frac{J^2|\langle n|\xi\rangle|^2|\langle k|\xi\rangle|^2}{E_n^{(0)} - E_k^{(0)}} + O(J^3). \quad (72)$$

The second order energy corrections cancel out in Eq. (71) due to the symmetric distribution of  $H_0$  eigenvalues. And the phase matches when the evolution time  $\tau$  becomes odd multiple of

$$\tau_{\text{CZ}} = \frac{\pi/J}{|\tilde{t}|^2 - |\tilde{s}|^2}, \quad (73)$$

where  $\tilde{t} = t/t_0$  and  $\tilde{s} = s/t_0$ . After explicitly setting the global and local phase factors to satisfy  $\phi_0 = -\delta E_1\tau_{\text{CZ}}$ ,  $\phi_0 + \phi_R = -\delta E_2\tau_{\text{CZ}}$  and  $\phi_0 + \phi_L = -\delta E_3\tau_{\text{CZ}}$ , we have the phase of  $\text{diag } \tilde{U}_{\text{major}}$  matches that of  $\text{CZ}[\phi]$ . The corresponding local phase corrections are found to be

$$\begin{aligned} \phi_L &= \pm \frac{\pi}{2} \left[ 1 + \frac{J}{4\varepsilon_Z} \frac{2(2+\delta)|\tilde{t}|^4 + \delta(2+\delta)|\tilde{s}|^4 + 8\delta|\tilde{s}|^2|\tilde{t}|^2}{4\delta(2+\delta)(|\tilde{t}|^2 - |\tilde{s}|^2)} \right], \\ \phi_R &= \pm \frac{\pi}{2} \left[ 1 - \frac{J}{4\varepsilon_Z} \frac{2(2-\delta)|\tilde{t}|^4 - \delta(2-\delta)|\tilde{s}|^4 - 8\delta|\tilde{s}|^2|\tilde{t}|^2}{4\delta(2-\delta)(|\tilde{t}|^2 - |\tilde{s}|^2)} \right], \end{aligned} \quad (74)$$

where the dimensionless factor  $\delta \equiv \delta\varepsilon_Z/\varepsilon_Z$ . The  $\pm$  signs in the front is '+' when  $|\tilde{t}| > |\tilde{s}|$  and '-' when  $|\tilde{t}| < |\tilde{s}|$ .

Assuming that those local phase corrections are accurately carried out, the gate fidelity is determined by the non-unity norm of the major part in addition to the minor part. Expressed in terms of gate infidelity, we have

$$\text{Inf}_{\text{CZ}} = \frac{1}{20} \left( \frac{J}{\varepsilon_Z} \right)^2 \left[ |\tilde{s}|^4 (1 - \cos(2\varepsilon_Z \tau_{\text{CZ}})) + \frac{4|\tilde{t}|^4}{\delta^2} (1 - \cos(\delta \varepsilon_Z \tau_{\text{CZ}})) \right. \\ \left. + \frac{32|\tilde{s}|^2|\tilde{t}|^2}{(2-\delta)^2} (1 - \cos(\varepsilon_Z(1 - \frac{\delta}{2})\tau_{\text{CZ}})) + \frac{32|\tilde{s}|^2|\tilde{t}|^2}{(2+\delta)^2} (1 - \cos(\varepsilon_Z(1 + \frac{\delta}{2})\tau_{\text{CZ}})) \right] + O\left(\frac{J}{\varepsilon_Z}\right)^4. \quad (75)$$

Our infidelity expression is only our best guess by the explicit construction routine specified earlier, but sufficient to approximate the analytical behavior of the true optimization results. We can further discard the oscillatory cosine parts and bound

$$\text{Inf}_{\text{CZ}} \lesssim \frac{1}{10} \left( \frac{J}{\varepsilon_Z} \right)^2 \left[ |\tilde{s}|^4 + \frac{4|\tilde{t}|^4}{\delta^2} + \frac{64(4+\delta^2)}{(4-\delta^2)^2} |\tilde{s}|^2 |\tilde{t}|^2 \right]. \quad (76)$$

In general, the gate-fidelity is not a monotonous function of the SOI strength. An possible effort for enhancing gate quality is to find a “sweet spot” where the RHS of Eq. (76) is kept as small as possible. To find the optimal working condition, we define the square-bracketed terms in the infidelity upper bound as  $\kappa$ . Through the relation  $|\tilde{s}|^2 + |\tilde{t}|^2 = 1$ , we can write  $\kappa$  as a function of  $\delta > 0$  and  $x \equiv |\tilde{s}|^2 \in [0, 1]$ :

$$\kappa = x^2 + \frac{4(1-x)^2}{\delta^2} + \frac{64(\delta^2+4)x(1-x)}{(\delta^2-4)^2}. \quad (77)$$

After taking the first and second order derivatives with respect to  $x$ , we find that  $\kappa$  attains minimum at either  $x = 0$  or  $x = 1$ . Combined with the definition that  $\tilde{s} = -i \sin \gamma_{\text{SO}} \sin \vartheta$ , This suggests that the gate infidelity achieves minima either when SOI is absent ( $\gamma_{\text{SO}} = 0$ ) or when  $\vartheta = \pi/2$  and  $\gamma_{\text{SO}} = (k - \frac{1}{2})\pi$ , namely, at an SOI node. Explicitly, for the case without SOI, we have

$$\text{Inf}_{\text{CZ}}(\gamma_{\text{SO}} = 0) \lesssim \frac{2}{5} \left( \frac{J}{\delta E_Z} \right)^2, \quad (78)$$

where we used the normal Zeeman energy here since  $f_{\text{SO}} = 1$ . This suggests that to achieve high-fidelity CZ gate in material with weak SOI such as silicon, it is required to have a relatively large difference in the effective magnetic field across quantum dots. While at the  $k$ th SOI node,

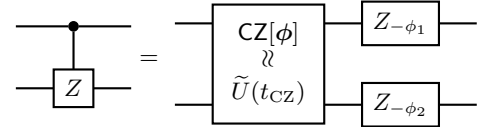
$$\text{Inf}_{\text{CZ}}(\gamma_{\text{SO}} = (k - \frac{1}{2})\pi) \lesssim \frac{1}{10} \left( \frac{J}{f_{\text{SO}} E_Z} \right)^2 \\ = \frac{1}{10} \left( \frac{J}{E_Z} \right)^2 \exp \left[ \frac{(2k\pi - \pi)^2}{8(d/x_0)^2} \right]. \quad (79)$$

It appears as if  $f_{\text{SO}}$  is playing the role of magnetic field gradient  $\delta$  here.

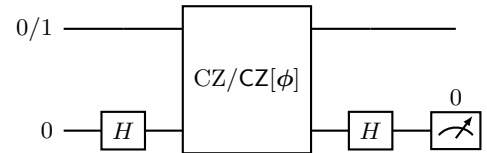
### C. Local phase measurements

In practice, the  $\text{CZ}[\phi]$  gate can be approximately implemented by turning on some coupling Hamiltonian for a specific period of time. As illustrated in Fig. 3a, this produces the standard CZ gate when combined with local phase corrections on individual qubits either before or after  $\text{CZ}[\phi]$ . While the global phase factor is unobservable, the local phase corrections are important for an accurate CZ. Consider for example the circuit in Fig. 3b, where the upper and lower line represents the control and target qubit. A standard CZ outputs target state  $|0\rangle$  for the control  $|0\rangle$  and  $|1\rangle$  for the control  $|1\rangle$ , which means that the measurement on the second qubit has full visibility—it’s  $|0\rangle$  and  $|1\rangle$  with 100% possibility. This is not the case if the CZ gate has not been locally phase-corrected. Say we send the first and second qubit to the upper and lower line, the possibility for measuring a  $|0\rangle$  state on the target qubit would be:

$$P(\text{target} = |0\rangle) = \begin{cases} \cos^2(\phi_2/2), & \text{control} = |0\rangle \\ \sin^2(\phi_2/2), & \text{control} = |1\rangle \end{cases}. \quad (80)$$



(a) The circuit implementation of CZ.



(b) The circuit to determine local phases.

FIG. 3: Implementing CZ and testing local phase.

This experimental setup can be used as a protocol to measure the phase correction  $\phi_2$  if it is not known in advance. Conversely, by exchanging the control and target qubit,  $\phi_1$  can also be measured in a similar fashion.

- 
- [1] V. N. Golovach, M. Borhani, and D. Loss, [Physical Review B](#) **74**, 165319 (2006).      [2] R. Li, J. Q. You, C. P. Sun, and F. Nori, [Physical Review Letters](#) **111**, 086805 (2013).